Kinesin rotates unidirectionally and generates torque while walking on microtubules

Avin Ramaiya[a,1], Basudev Roy[a,1,2], Michael Bugiel[a], and Erik Schäffer[a,3]

[a]Cellular Nanoscience, Center for Plant Molecular Biology, University of Tübingen, 72076 Tübingen, Germany

Edited by J. Richard McIntosh, University of Colorado, Boulder, CO, and approved August 22, 2017 (received for review April 26, 2017)

Cytoskeletal motors drive many essential cellular processes. For example, kinesin-1 transports cargo in a step-wise manner along microtubules. To resolve rotations during stepping, we used optical tweezers combined with an optical microprotractor and torsion balance using highly birefringent microspheres to directly and simultaneously measure the translocation, rotation, force, and torque generated by individual kinesin-1 motors. While, at low adenosine 5′-triphosphate (ATP) concentrations, motors did not generate torque, we found that motors translocating along microtubules at saturating ATP concentrations rotated unidirectionally, producing significant torque on the probes. Accounting for the rotational work makes kinesin a highly efficient machine. These results imply that the motor's gait follows a rotary hand-over-hand mechanism. Our method is generally applicable to study rotational and linear motion of molecular machines, and our findings have implications for kinesin-driven cellular processes.

kinesin | optical tweezers | polarization microscopy | birefringence | rotation

Kinesin-1 is a dimeric, ATP-driven molecular machine transporting vesicular cargo (1–3) while stepping in a hand-over-hand fashion (4–7) along microtubules. Because of the identical subunits, the motor has been proposed to rotate unidirectionally during stepping, implying that the tail of motors and vesicles will tend to wind up and spin (8). However, experiments done at low ATP concentrations only revealed occasional, random motor rotations (9, 10). An asymmetry in the timing of consecutive steps, so-called limping (5, 11), was interpreted as an alternation in the rotation direction of consecutive steps and later attributed to loads perpendicular to the microtubule axis (12, 13). However, direct evidence for any rotational motion, in particular at high, physiological ATP concentrations, is lacking.

Optical tweezers are versatile tools used for either force or torque spectroscopy applied to investigate the translation or rotation of molecular machines, respectively (14, 15). However, methods to simultaneously measure linear and rotational motion with molecular resolution are scarce. Here, we introduce a rotation detector to an optical trap using liquid crystalline microspheres that are stable in aqueous solutions, can be easily varied in size, and can be functionalized with biomolecules. We applied the method to measure translational and rotational degrees of freedom of single kinesin motor proteins at the same time.

Results

Torsional Stiffness of Kinesin. If motors rotated and were able to transfer torque onto cargo, motors should be rigid and have a rotational stiffness. To measure the rotational stiffness of kinesin, we coupled birefringent microspheres (*SI Appendix*, Fig. S1) to single kinesin-1 motors (Fig. 1 and *Materials and Methods*). The two kinesin-1 motor heads are linked by a coiled coil, the stalk, which is interrupted by so-called hinge domains (8). These hinges may switch between a folded and unfolded state and are thought to provide torsional flexibility (10, 16, 17). Because rotational compliance increases with length, we used a short, recombinant, GFP-labeled rat kinesin-1 truncated after the first hinge domain (Fig. 1*A*). Via anti-GFP antibodies, we bound the motors to microspheres composed of an ordered liquid crystal RM257 (18–20) with a birefringence of 0.18, 20 times larger compared with that of quartz cylinders commonly used in optical torque wrenches (21–23). This high birefringence enables high contrast in polarization microscopy and a fast response time in angular trapping applications (19). For rotation detection, we coupled these microspheres to kinesin motors and confirmed that single motors were functional after the coupling procedure (*Materials and Methods*). To test whether both the motor head–microtubule and, in particular, the motor stalk–microsphere linkage are rotationally constrained and can sustain torque, we twisted motors and observed their recoil response. In this experiment, we used the nonhydrolyzable ATP analogue adenylyl imidodiphosphate (AMP-PNP). When AMP-PNP is bound to motors, they are thought to be in the two-heads-bound state mimicking the predominant motor conformation at high ATP concentrations. To observe the angular orientation of the microsphere, we used polarization microscopy. To set the initial rotation state, we used the optical tweezers. We placed motor-coupled microspheres under single-molecule conditions on microtubules using a linearly polarized laser trap (Fig. 1*B*, *Inset*, *SI Appendix*, Fig. S2, and *Materials and Methods*). We twisted the motor by rotating the trapping laser polarization by 45° to the extinction position of the polarization microscope. Since the extraordinary axis of the microsphere aligns with the polarization direction (21), the microsphere is rotated by this angle. Subsequently, we turned the trap off. Using solely the polarization microscopy contrast, we observed that the microsphere brightness, quantified by an

Significance

Given the importance of cytoskeletal motor proteins, we asked whether translational motors rotate while walking along their tracks. Using an optical tweezers-based approach, we simultaneously measured translation, force, rotation, and torque of a kinesin motor with molecular resolution. We found that the gait followed a rotary stepping mechanism that generates torque and spins cargo. Thus, during walking, the motor "tail (and organelle) will tend to wind up like the rubber band of a toy airplane," as Joe Howard hypothesized in 1996. To determine the overall motor efficiency, our measurements also point to the importance of accounting for rotational work. Apart from other cytoskeletal motors, the technique may be applied to molecular machines such as DNA motors and rotary engines like the ATP synthase.

Author contributions: E.S. designed research; A.R., B.R., and M.B. performed research; A.R., B.R., M.B., and E.S. analyzed data; and A.R., B.R., and E.S. wrote the paper.

The authors declare no conflict of interest.

This article is a PNAS Direct Submission.

[1]A.R. and B.R. contributed equally to this work.

[2]Present address: Department of Physics, Indian Institute of Technology, Madras 600036, India.

[3]To whom correspondence should be addressed. Email: Erik.Schaeffer@uni-tuebingen.de.

This article contains supporting information online at www.pnas.org/lookup/suppl/doi:10.1073/pnas.1706985114/-/DCSupplemental.

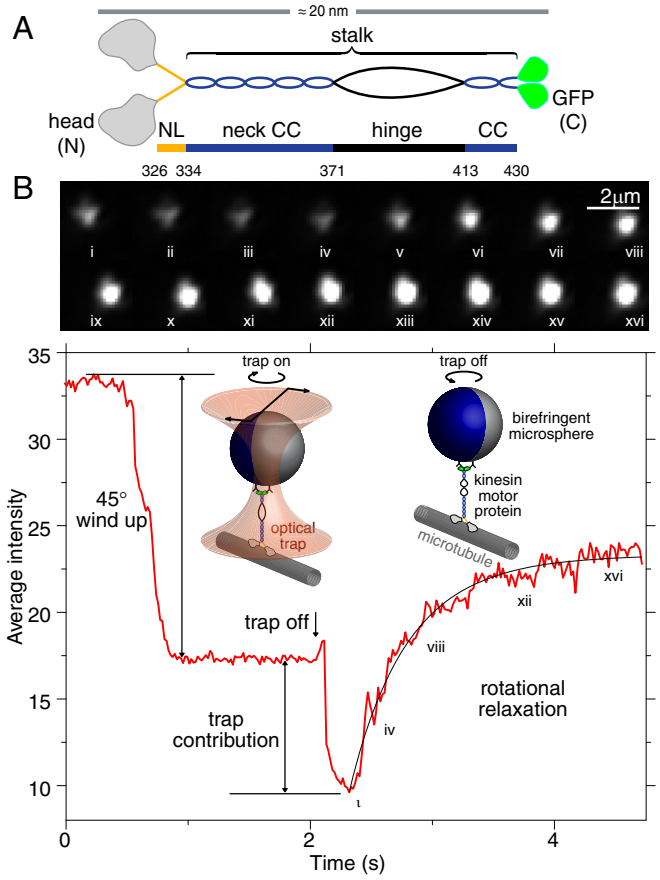

Fig. 1. Kinesin structure and twisting of a motor coupled to a birefringent microsphere. (*A*) The rat kinesin-1 homodimer consists of two N-terminal motor heads, neck linkers (NL, orange), a hinge domain (black), two coiled-coil domains (CC, blue; the first one is also called neck) truncated after amino acid 430, and C-terminally tagged GFP (green). (*B*) Polarization microscopy. (*Top*) Image sequence of a rotating, motor-attached birefringent microsphere with radius $R = 0.65 \pm 0.04$ μm viewed under crossed polarizers in AMP-PNP (time between frames: 136 ms). (*Bottom*) Average microsphere image intensity I vs. time t (red line). The relaxation was fitted to $I \propto \sin^2(\frac{\pi}{2}\{1 - \exp[-(t - t_0)/t_{\rm rot}]\})$ with an offset t_0 and $t_{\rm rot} = 0.98 \pm 0.05$ s (black line). (*Inset*) Illustration of the twisting experiment. Schematics are not drawn to scale.

average intensity over a region of interest around the microsphere, increased again (Fig. 1*B*). This increase is consistent with a rotation back to the initial microsphere orientation. A control measurement confirmed the expected image intensity dependence on the rotation angle (*SI Appendix*, Fig. S3). For the twisted kinesin, the slow rotation back to the initial state was well described by an exponential function (black line in Fig. 1*B*) with a relaxation time constant $t_{\rm rot} = \gamma/\kappa_{\rm motor}$, where $\gamma = 8\pi\eta R^3\lambda$ is the rotational drag coefficient, with $\lambda \approx 1.12$ accounting for the surface proximity (ref. 24 and *SI Appendix*, section 1). Using the known viscosity η and microsphere radius R, we determined the torsional stiffness $\kappa_{\rm motor} = \gamma/t_{\rm rot}$ of the motor to be 4.0 ± 0.5 pN nm·rad^{-1} (SEM unless stated otherwise, $N = 9$), consistent with reported values (10, 17). Thus, motors have a torsional stiffness large enough to support and transfer torque.

Kinesin Generates Torque. To test whether motors could generate torque during translocation, we performed a motility assay with motor-coupled microspheres powered by single motors under high ATP concentrations (1 mM, Fig. 2). Here, we used the optical tweezers only as a helping device to place a microsphere on a microtubule. Then, we turned off the trap and recorded an image sequence using polarization microscopy. During the translocation, the microsphere brightness changed (Fig. 2*A*). Using pattern matching, we tracked the microsphere and plotted its position and intensity, determined as above, as a function of time (blue and red lines, respectively, Fig. 2*B*). The intensity change is consistent with a constant rotation rate of the microsphere (black line, Fig. 2*B*), implying that the motor was able to generate a torque sufficient to continuously and unidirectionally rotate the microsphere. Thus, in the absence of the optical trap, this experiment shows that the motor can generate significant torque at high ATP concentrations.

Kinesin Rotates Unidirectionally. How is torque generated? To achieve a molecular resolution, we used optical tweezers combined with a rotation detector based on the backscattered trapping light—an optical microprotractor and torsion balance (*SI Appendix*, Fig. S2). Using a force clamp (25) and a high ATP concentration (1 mM), we could independently record both translational and rotational motion (*SI Appendix*, Fig. S4*A*). In contrast, at a low ATP concentration (1 μM), we did not measure a significant rotation signal (*SI Appendix*, Fig. S4*B*). This absence of rotations is consistent with the notion that the motor is strongly bound only by one head at low ATP concentrations (26, 27) that is not able to sustain torque for extended periods. To quantify the rotation and torque, we calibrated the backscattered laser intensity signal of a birefringent microsphere trapped with an elliptically polarized laser adapting our combined power spectral density–drag force calibration method (28, 29) for rotations (*Materials and Methods* and *SI Appendix*, section 1 and Fig. S6). The ellipticity was important for a linear response of the detector (*SI Appendix*, section 1). After we determined the angle sensitivity and torsional stiffness, we placed the motor-coupled microspheres on microtubules and recorded the position, force, angle, and torque of the microsphere (Fig. 3). Surprisingly, at sufficiently high ATP concentrations ($\gtrsim$50 μM), single motors simultaneously displaced the birefringent microspheres from the trap center and rotated them in a step-wise fashion (blue and red lines, respectively, in Fig. 3 *A* and *B* and *SI Appendix*, Fig. S7). Detected angular steps were small ($\sim 1^\circ$) because the optical trap acts like a torsion balance with a much larger optical

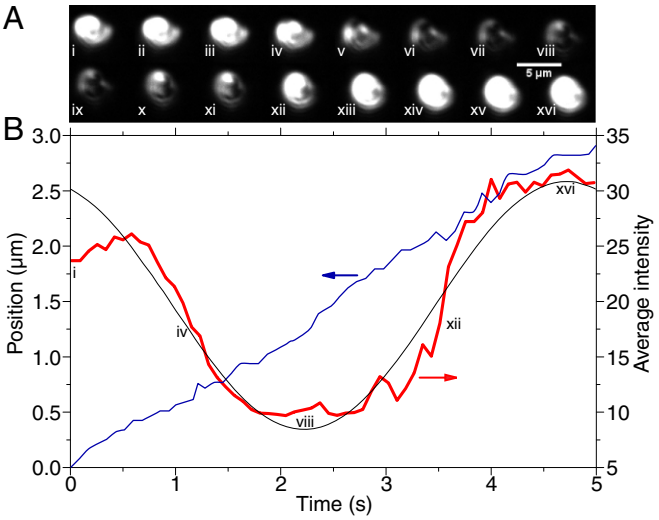

Fig. 2. Motility of a single, kinesin-driven, birefringent microsphere imaged using polarization microscopy without the optical trap. (*A*) Image sequence with 340 ms between displayed frames. The microsphere radius was 2.10 ± 0.05 μm. (*B*) Microsphere position (blue line) and average intensity per pixel (red line) of the images in *A* as a function of time. A sinusoidal line (black) is drawn as a guide to the eye.

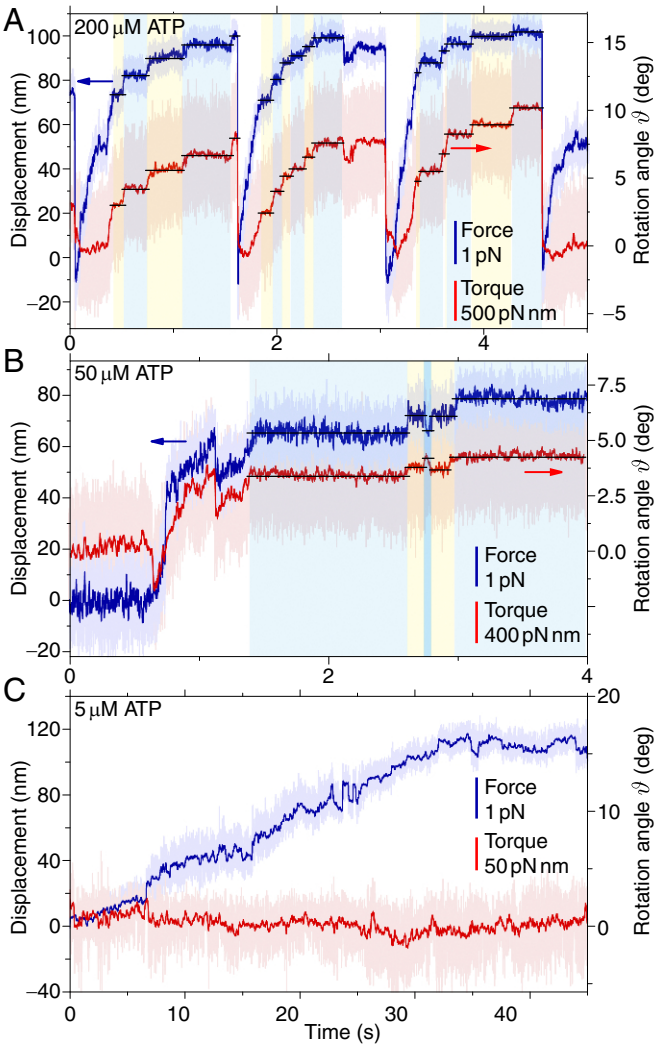

Fig. 3. Motility and rotation of motor-driven, birefringent microspheres in the optical tweezers combined with the optical microprotractor and torsion balance. The displacement (blue line, left-hand axis) and angle (red line, right-hand axis) are plotted as a function of time. Static trap data are recorded with an ATP concentration and microsphere diameter of (*A*) 200 μM and 0.64 μm, (*B*) 50 μM and 1.06 μm, and (*C*) 5 μM and 0.60 μm, respectively. Yellow and blue shaded regions indicate simultaneous rotational and translational steps. Black lines indicate their mean values.

torsional stiffness κ_{trap} compared with that of the motor ($\kappa_{\text{motor}} \ll \kappa_{\text{trap}}$). Thus, for a balanced torque $\tau_{\text{optical}} = \tau_{\text{motor}}$ corresponding to $\kappa_{\text{trap}}\vartheta_{\text{protractor}} = \kappa_{\text{motor}}\vartheta_{\text{motor}}$, the motor turns by a much larger angle $\vartheta_{\text{motor}} = (\kappa_{\text{trap}}/\kappa_{\text{motor}})\vartheta_{\text{protractor}}$ compared with the change in the microsphere angle. The large optical torsional stiffness together with the small angular steps enabled a fast response time for resolution of motor rotations at high ATP concentrations. For a specific microsphere, rotations were mostly unidirectional. Out of 21 microspheres, 8 showed right-handed and 13 showed left-handed rotations when looking in the translation direction (positive and negative rotation signals, respectively). Based on a binomial distribution, the handedness was not significantly different from an equal probability to either turn leftward or rightward. Displacing the microsphere perpendicular to the microtubule axis did not affect the rotation direction (*SI Appendix*, Fig. S8 and section 4). Presumably, the directionality for a microsphere is established by how the motor is bound both with respect to its angular orientation and position relative to the extraordinary axis of the microsphere or by the location of the microtubule protofilament, on which the motor walks, relative to the middle of the microtubule. Interestingly, we observed that, for a translational backward step at 2.7 s, in Fig. 3*B*, the angular step was still positive (see also *SI Appendix*, Fig. S8). Only for the next forward step, the angular step was negative, indicating a reversal of the motor rotation direction. As in the force-clamp experiments, motors did not generate any torque at low ATP concentrations (5 μM, Fig. 3*C*). Thus, our data indicate that, at a sufficiently high ATP concentration, torque is incrementally generated in a step-wise manner by a mostly unidirectional rotation of the motor.

Kinesins Perform Rotational Work and Are Highly Efficient. Do the motors perform significant rotational work? Motors generated force up to about 5 pN and torque up to about $\tau_{\text{max}} \approx 1{,}650$ pN nm (Fig. 3). When motors approached the stall force, both the displacement and angular traces showed discrete steps. To determine the time points at which positional steps occurred, we used an unbiased step detector (30) (blue and yellow shaded regions in Fig. 3). To quantify the angular steps, we averaged the angular trace over the dwell time of the positional steps and marked, with black lines, the average position and angle during a dwell. Individual angular steps $\vartheta^{\text{step}}_{\text{protractor}}$ concurrent with displacement steps were, on average, $1.1 \pm 0.2°$ ($N = 20$). Alternate step durations close to stall forces differed significantly, indicating that motors limped (*Materials and Methods*). In the torsion balance, the motor torque is equal to the optical torque. Thus, the angular steps correspond to an increase in torque per step of $\tau^{\text{step}}_{\text{motor}} = \tau^{\text{step}}_{\text{optical}} = \kappa_{\text{trap}}\vartheta^{\text{step}}_{\text{protractor}} = 170 \pm 20$ pN nm ($N = 20$). Since the motor must turn by $\vartheta^{\text{step}}_{\text{motor}} = 180°$ per step (8), we calculated the torsional stiffness of the motor to be $\kappa_{\text{motor}} = \tau^{\text{step}}_{\text{motor}}/\pi = 54 \pm 7$ pN nm·rad^{-1} (propagated SEM). This torsional stiffness is significantly larger compared with the one measured for the 45° relaxation in AMP-PNP (Fig. 1*B*), indicating a torsional stiffening of the motor. Such stiffening may be due to a windup and stretching of the stalk with increasing load. For many traces, we only observed significant rotation signals starting after a microsphere displacement of ∼50 nm or approximately six steps corresponding to three full turns (see, e.g., Fig. 3*A*). This supertwist and windup in the motor stalk may cause the torsional stiffening. Higher torsional motor stiffness states have also been reported previously (figure S3 in ref. 10). The maximum translational work—the maximum force times the translational step size—was 45 ± 5 pN nm ($N = 6$), and the maximum rotational work—the maximum torque (τ_{max}) times the angular step size ($\vartheta^{\text{step}}_{\text{protractor}}$)—was 32 ± 15 pN nm ($N = 6$, SEM of ±3 pN nm plus ±12 pN nm for retardance correction; see *SI Appendix*, section 2). Thus, the total work per step performed by the motor was up to 77 ± 16 pN nm (propagated error). Dividing by the free energy available per hydrolysis of 1 ATP molecule of ∼100 pN nm (8) results in an overall efficiency—when accounting for both translational and rotational work of the motor—of about 80%, making it a highly efficient molecular machine, much higher than previously thought.

Discussion

The rotation and generation of torque have implications for the structure and the stepping mechanism. Recent work on intermediate states during stepping is consistent with continuous, unidirectional motor rotations (31, 32), supporting our findings. A torsional stiffening of the motor under load and potential supertwisting may be due to a structural rearrangement of the hinge domain in the motor stalk (17). Unfolding of the hinge domain might be necessary to twist the motor by multiple turns. Furthermore, our findings that the motor can sustain large torque imply that, during stepping, the bottom of the motor stalk, i.e., the position at which the neck linkers connect to the neck coiled

coil, must be torsionally constrained. Otherwise, during stepping, when only one head is in a strongly bound state, the single polypeptide chain of the neck linker would allow free rotation, releasing the torque before the second head rebinds to the microtubule lattice. Therefore, either the neck linker must be docked up to the start of the neck coiled coil or, our favored hypothesis, the advancing head is not freely moving through space to its next binding site. In the latter case, the head should be directly guided on the microtubule lattice next to the other motor head from one binding site to the next, for example, by electrostatic interactions (33). Directly next to the other head, there might be a local potential minimum corresponding to a docked or intermediate state (27, 31, 32, 34). We observed that the motor could slide backward on the microtubule lattice without a change in the rotation angle and confirmed that motors did not detach from the microtubule lattice during sliding, by imposing upward loads on the motors (*SI Appendix*, section 3 and Figs. S7 and S18). Such sliding motion supports the idea of a continuous electrostatic guidance track for both heads on the microtubule lattice. When the motor switches to a truly one-head-bound state without contact of the second head with the microtubule lattice, torque is released by a fast swiveling motion around the neck linker of the bound head. Such events would correspond to previously reported occasional stalk reversals (10). Thus, we propose to refine the notion of a one-head-bound state that one head is strongly bound and the other weakly bound, able to diffuse in a one-dimensional well along the microtubule lattice. Only occasionally, the weakly bound head fully detaches, resulting in a truly one-head-bound state. Such a refined state is consistent with previous work (9, 26, 27). Since, most of the time, both heads are in contact with the microtubule lattice in such a state, the motor appears to be torsionally stiff (9, 10). However, a larger torque cannot be sustained, because of occasional stalk reversals. With decreasing ATP concentrations, our data imply a slow transition from the rotationally constrained pseudo-one-head-bound state to the canonical rotationally unconstrained one-head-bound state in the sense that the probability to be in the latter state increases. How torque generation of the kinesin dimer is related to torque generation of ensembles of single-headed kinesins and asymmetric force-dependent sideward stepping of dimeric kinesins is unclear at the moment (35–38). Together, our data support the notion that kinesin steps with a rotary hand-over-hand mechanism most likely being asymmetric because motors also limped. Limping is still consistent with a rotary hand-over-hand mechanism, because the effect is attributed to an independent degree of freedom, i.e., to different vertical loads on the heads in successive steps—originating from a $\sim 120^\circ$ instead of a 180° rotational symmetry of an unbound dimer (39)—and possibly "breathing" of the last heptad repeat of the neck coiled coil (12, 13).

In cells, the rotation of the motor implies that torque should be transferred to cargo and might be buffered by the hinge domain and remaining stalk of full-length motors. Because we observed slow rotations for large cargo (Fig. 2) and motor rotations were often detected after a lag phase, we expect that torque corresponding to several turns of the motor stalk can be taken up by the motor, most likely having a nonlinear torsional stiffness. Due to the torsional stiffness, the motor has the ability to transfer torque. Therefore, kinesin-transported vesicles should rotate. Torsion might be relieved by a rotation of the motor's tail in the fluid membrane of the vesicle (8). When motors cross-link microtubules for relative sliding (40), torque should be exerted on the microtubules, and occasional stalk reversals (10) may be required to prevent overwinding of motors. Thus, a large torque may affect the dynamics of transport and other kinesin-mediated processes. In general, our optical microprotractor and torsion balance can be applied to simultaneously measure translation and rotation of a wide range of molecular machines, including cytoskeletal motors, rotary engines like the bacterial flagellar or pili motors and the ATP synthase, or DNA topoisomerases. Rotations and the generation of torque may have to be considered for other kinesin and cytoskeletal motors and the rotational work accounted for to determine the overall motor efficiency.

Materials and Methods

Kinesin Expression and Purification. We used truncated rat kinesin-1 rK430 (kinesin heavy chain isoform 5C from *Rattus norvegicus*) with a C-terminal GFP and hexa-histidine tag. The protein was expressed from a bacterial plasmid PET-17b with an ampicillin selection marker. The cloned plasmid was originally provided to us by the Howard Laboratory, Yale University, New Haven, CT. Briefly, using heat shock, the cloned plasmid was transformed into Bl21(DE3)pRARE *Escherichia coli* competent cells. The bacteria were grown as a small culture in lysogeny broth and plated onto agar plates with ampicillin. Growing bacteria were selected for further growth in 700 mL of warm AMP-LB medium until the medium had an optical density of 0.8. The bacteria were then induced using isopropyl β-D-1-thiogalactopyranoside and allowed to grow for 12 h. The bacteria were centrifuged, and the pellet was lysed using a tip sonicator in a cold room for 60 s (6 × 10-s pulses with 20-s intervals). Then, the lysate was centrifuged to separate proteins from the cellular debris. The supernatant postcentrifugation was passed through a 1-mL HisTRAP column (17.5247.01; GE Healthcare) at a flow rate of 1 mL/min. The protein was eluted using 300 mM imidazole in the elution buffer.

Synthesis of Birefringent Microspheres. Birefringent microspheres were synthesized by evaporation and precipitation of the nematic liquid crystal precursor RM257 (Merck). The protocol is described in refs. 18 and 20 and schematically illustrated in *SI Appendix*, Fig. S1. Briefly, RM257 was added as a white amorphous powder to prewarmed (55 °C) ethanol with a mass-to-volume ratio of 0.1 to 1 mg/mL resulting in about 0.2- to 5-μm-diameter microspheres. To completely dissolve RM257, the solution was stirred with a magnetic stirrer at 55 °C. Simultaneously, in a separate beaker, a 3:1 solution of water and ethanol was heated to 75 °C. Subsequently, 10× the weight of RM257 of the photoinitiator Darocur 1173 (BASF) was added to the RM257 solution. The RM257 solution was then immediately transferred dropwise to the water–ethanol solution with continuous heating (75 °C) and stirring of the solution. The water–ethanol solution volume was 10-fold that of the RM257 solution. The mixture was heated until the entire volume of ethanol evaporated. Birefringent microspheres precipitated during this stage while the solution turned milky. The size of the birefringent microspheres was controlled by varying the initial RM257 concentration, the ethanol–water ratio, and the evaporation rate.

Acrylate Coupling of Antibodies and Motor Protein Attachment. For protein coupling, 200 μL of birefringent microspheres with an approximate concentration of 10^{10} microspheres per milliliter in deionized water were supplemented with 100 μL of 10 μM monofunctional methoxy-PEG-acrylate molecules (2 kDa molecular weight, Creative PEGworks) in borate buffer (pH 8.5), and 1 μL of 30 μM N-acryloxysuccinimide (Sigma) in DMSO and incubated on ice for 5 min. Then, we added 100 μL BRB80 (80 mM piperazine-*N*,*N*′-bis(2-ethanesulfonic acid)/KOH pH 6.9, 1 mM $MgCl_2$, 1 mM EGTA) and, for activation, irradiated the solution with UV light (ULTRAVITALUX ultraviolet high-pressure lamp; OSRAM) for 20 s at a distance of 15 cm. Immediately afterward, 5 μL of 6.4 mg/mL anti-GFP antibody (monoclonal from mice, antibody facility Max Planck Institute of Molecular Cell Biology and Genetics) was added, and the solution was incubated for 2 h on ice. The antibody-coupled microspheres were incubated with the appropriate rK430 concentration [$\sim$10,000× diluted stock concentration of 100 μM for single-molecule conditions (41)] for 8 min at room temperature and then diluted in motility buffer (BRB80-taxol with 0.5 mg/mL casein, ATP of appropriate concentration, and an antifade mixture [0.5% β-mercaptoethanol, 20 mM glucose, 20 μg/mL glucose oxidase, 8 μg/mL catalase, 10 mM DTT]).

Microtubule, Flow Cell, and Motility Assay Preparation. Kinesin-coated microsphere assays were performed in flow cells. Flow cells with immobilized microtubules were constructed and prepared as described in ref. 30.

Motor Functionality Under Single-Molecule Conditions. To confirm that motors were functional after coupling, we placed motor-coupled microspheres onto surface-immobilized microtubules using the optical tweezers. After turning off the trap, we tracked the microsphere motion using differential interference contrast with an LED illumination (LED-DIC). To ensure single-molecule conditions, only about one out of five microspheres

showed motility (3). At a temperature of 29.2 °C (42), we measured a microsphere speed of 0.85 ± 0.11 μm/s ($N = 19$) consistent with the motor speed of 0.95 ± 0.07 μm/s measured by single-molecule fluorescence microscopy without microspheres and literature values (2, 3). The agreement confirmed the functionality of the motor when attached to a birefringent microsphere.

Optical Tweezers, Optical Microprotractor, Torsion Balance, and Polarization Microscopy. The measurements were performed in a single-beam optical tweezers combined with LED-DIC microscopy to visualize single microtubules. The setup, schematically depicted in *SI Appendix*, Fig. S2, and calibration procedures for translation and force measurements were described in detail earlier (29, 42, 43). Briefly, the setup has near-angstrom resolution in surface-coupled assays, is equipped with a millikelvin precision temperature control on the trapping objective set to 29.200 °C, and has a 3D force feedback using piezo tilt mirrors for the lateral and a piezo translation stage for the axial direction (25). For polarization microscopy, we removed the DIC prisms. The polarization direction of the visible illumination is rotated 45° relative to the trapping laser polarization. Thus, when viewed under crossed polarizers, trapped microspheres have maximum brightness. For rotation measurements, we added a half-wave and sometimes additionally a quarter-wave plate before the trapping objective to adjust the laser polarization state. In addition, we introduced a polarizing beam splitter (PBS) to couple out the backscattered laser light onto a photodiode (QP45-Q TO, operated at 50 V reverse bias; First Sensor AG). We call the light intensity measured by this rotation detector a "rotation signal." For circular polarization, the backscattered light reverses its polarization direction and, after passing the quarter-wave plate, is linearly polarized, with a polarization direction perpendicular to the incoming light. Thus, the photodiode after the PBS detects all backscattered light if the reflection did not result in elliptical polarization. The intensity of the rotation signal depends on the orientation of the microsphere and has the same twofold rotational symmetry as the microsphere. Therefore, the signal is proportional to $\sin(2\theta)$, where θ is the rotation angle of the microsphere. As expected (21), when we used a circularly polarized laser for trapping in our optical tweezers, these microspheres rotated (*SI Appendix*, Fig. S9). For linear polarization, the backscattered light intensity that reaches the photodiode is proportional to $\sin^2(\vartheta)$, where ϑ is the angle between the microsphere's extraordinary axis and the laser polarization direction. This angular dependence also results in a twofold rotational symmetry. Importantly, to achieve a linear response of the rotation signal as a function of ϑ, the trapping light needs to have elliptical polarization. We rotated the major axis by 20° compared with the system's orthogonal coordinate system and microtubule axis (see *SI Appendix*, section 1). All stationary trap measurements were performed in this configuration. To calibrate the rotation signal for the case of elliptical polarization, we first calibrated the parameters for translation and force measurements (29). We measured the lateral displacement sensitivity, trap stiffness, and, importantly, the microsphere's translational drag coefficient. From the latter, we determined the microsphere radius, which we use as an input for the rotational calibration. We recorded a power spectrum of the rotational Brownian motion (*SI Appendix*, Fig. S6) and determined the angle sensitivity and torsional stiffness of the trap using the known microsphere radius and thus the known rotational drag coefficient (see *SI Appendix*, section 1). For polarization microscopy, images were recorded with 59 frames per second. Trapping time traces were recorded at 40 kHz with an alias-free analog-to-digital converter. Traces were smoothed with a running median filter with a bandwidth of 200 Hz. We corrected for the nonlinear response of the rotation detector (*SI Appendix*, sections 1 and 2) and a small crosstalk between translation and rotation signals corresponding to <4% per step (*SI Appendix*, Fig. S10). Some microspheres got stuck after experiments, which was beneficial to determine the crosstalk directly by scanning through the immobilized microspheres. For microspheres that remained mobile, we subtracted an average 0.8% of crosstalk between the translation and rotational signals from the raw voltage data. The force clamp was operated with an update rate of 500 Hz. The diameter of the birefringent microspheres used in the motility trapping experiments ranged from about 0.6 μm to 1.2 μm, with an average size of about 0.95 μm, an average trap stiffness of 0.051 pN/nm, and an average torsional stiffness of 9,200 pN nm/rad. In the torsion balance mode using a 600-nm-diameter microsphere with the average torsional stiffness, we could resolve angular steps of 1° with a signal-to-noise ratio of 5 at a bandwidth of 100 Hz. The corresponding root-mean-square, angular resolution $\sigma_\vartheta = [\kappa_{\mathrm{trap}}]^{-1}(2k_B T\gamma/t_{\mathrm{meas}})^{1/2}$ for a measurement time t_{meas} of 1 ms and 10 ms was 0.7° (12 mrad) and 0.2° (3.8 mrad), respectively. Overall, we analyzed the motion of 322 different microspheres interacting with 319 different microtubules on 43 different days; 65 out of 322 microspheres showed motility (20%), and 57 out of these 65 showed simultaneous translation and rotation (88%). Clear simultaneous steps in both translation and rotation signals were observed for 12 microspheres. For low ATP concentrations (≤5 μM), 8 out of 33 microspheres (24%) showed motility. While all eight microspheres showed displacement activity, none showed any rotation signal. To calculate the limping ratio, we used all consecutive steps for which forces were larger than 4 pN, i.e., close to stalling conditions, and for which clear steps in both translation and rotation were visible. The resulting $N = 45$ angular steps that met the criteria were obtained from seven different microspheres. The average dwell time of the short and long steps were significantly different at the 95% confidence level and were 0.32 ± 0.05 s ($N = 22$) and 0.64 ± 0.14 s ($N = 23$) long, respectively. These values resulted in a limping ratio of 2.0 ± 0.5.

ACKNOWLEDGMENTS. This work is dedicated to Joe Howard for his mentoring, contribution to the kinesin field, and his 60th birthday. This manuscript was based on a hypothesis he put forward in ref. 8. We thank J. Howard, K. Harter, M. Mahammdeh, M. Jahnel, V. Bormuth, A. Jannasch, G. Hermsdorf, and M. Chugh for comments on the manuscript. We thank K. Sandomirski and T. Gisler for a detailed protocol on how to make birefringent microspheres and N. Azadfar for help with the protein purification. A.R. thanks the Dresden International Graduate School for Biomedicine and Bioengineering for a PhD fellowship. B.R. thanks the Alexander von Humboldt Foundation for a postdoctoral fellowship. This work was supported by the Deutsche Forschungsgemeinschaft (Emmy Noether Program), European Research Council (Starting Grant 2010, Nanomech 260875), the Technische Universität Dresden, and the Universität Tübingen.

1. Vale RD, Reese TS, Sheetz MP (1985) Identification of a novel force-generating protein, kinesin, involved in microtubule-based motility. *Cell* 42:39–50.
2. Howard J, Hudspeth AJ, Vale RD (1989) Movement of microtubules by single kinesin molecules. *Nature* 342:154–158.
3. Block SM, Goldstein LSB, Schnapp BJ (1990) Bead movement by single kinesin molecules studied with optical tweezers. *Nature* 348:348–352.
4. Kaseda K, Higuchi H, Hirose K (2003) Alternate fast and slow stepping of a heterodimeric kinesin molecule. *Nat Cell Biol* 5:1079–1082.
5. Asbury CL, Fehr AN, Block SM (2003) Kinesin moves by an asymmetric hand-over-hand mechanism. *Science* 302:2130–2134.
6. Yildiz A, Tomishige M, Vale RD, Selvin PR (2004) Kinesin walks hand-over-hand. *Science* 303:676–678.
7. Schief WR, Clark RH, Crevenna AH, Howard J (2004) Inhibition of kinesin motility by ADP and phosphate supports a hand-over-hand mechanism. *Proc Natl Acad Sci USA* 101:1183–1188.
8. Howard J (1996) The movement of kinesin along microtubules. *Annu Rev Physiol* 58:703–729.
9. Hua W, Chung J, Gelles J (2002) Distinguishing inchworm and hand-over-hand processive kinesin movement by neck rotation measurements. *Science* 295: 844–848.
10. Gutiérrez-Medina B, Fehr AN, Block SM (2009) Direct measurements of kinesin torsional properties reveal flexible domains and occasional stalk reversals during stepping. *Proc Natl Acad Sci USA* 106:17007–17012.
11. Higuchi H, Bronner CE, Park H, Endow SA (2004) Rapid double 8-nm steps by a kinesin mutant. *EMBO J* 23:2993–2999.
12. Xie P, Dou SX, Wang PY (2007) Limping of homodimeric kinesin motors. *J Mol Biol* 366:976–985.
13. Fehr AN, Gutiérrez-Medina B, Asbury CL, Block SM (2009) On the origin of kinesin limping. *Biophys J* 97:1663–1670.
14. Lipfert J, van Oene MM, Lee M, Pedaci F, Dekker NH (2015) Torque spectroscopy for the study of rotary motion in biological systems. *Chem Rev* 115:1449–1474.
15. Gennerich A (2017) *Optical Tweezers: Methods and Protocols*, Methods in Molecular Biology (Springer, New York), Vol 1486.
16. Hunt AJ, Howard J (1993) Kinesin swivels to permit microtubule movement in any direction. *Proc Natl Acad Sci USA* 90:11653–11657.
17. Crevenna AH, et al. (2008) Secondary structure and compliance of a predicted flexible domain in kinesin-1 necessary for cooperation of motors. *Biophys J* 95:5216–5227.
18. Sandomirski K, Martin S, Maret G, Stark H, Gisler T (2004) Highly birefringent colloidal particles for tracer studies. *J Phys Condens Matter* 16:S4137–S4144.
19. Martin S, Reichert M, Stark H, Gisler T (2006) Direct observation of hydrodynamic rotation-translation coupling between two colloidal spheres. *Phys Rev Lett* 97:248301.
20. Jannasch A, et al. (2017) Custom-made microspheres for optical tweezers. *Optical Tweezers*, Methods in Molecular Biology, ed Gennerich A (Humana, New York) Vol 1486, pp 137–155.
21. La Porta A, Wang MD (2004) Optical torque wrench: Angular trapping, rotation, and torque detection of quartz microparticles. *Phys Rev Lett* 92:190801.
22. Deufel C, Forth S, Simmons CR, Dejgosha S, Wang MD (2007) Nanofabricated quartz cylinders for angular trapping: DNA supercoiling torque detection. *Nat Methods* 4:223–225.

23. Pedaci F, Huang Z, van Oene M, Dekker NH (2012) Calibration of the optical torque wrench. *Opt Express* 20:3787–3802.
24. Brenner H (1964) Slow viscous rotation of an axisymmetric body within a circular cylinder of finite length. *Appl Sci Res* 13:81–120.
25. Bugiel M, Jannasch A, Schäffer E (2017) Implementation and tuning of an optical tweezers force-clamp feedback system. *Optical Tweezers*, Methods in Molecular Biology, ed Gennerich A (Humana, New York), Vol 1486, pp 109–136.
26. Mori T, Vale RD, Tomishige M (2007) How kinesin waits between steps. *Nature* 450:750–754.
27. Guydosh NR, Block SM (2009) Direct observation of the binding state of the kinesin head to the microtubule. *Nature* 461:125–128.
28. Tolić-Nørrelykke SF, et al. (2006) Calibration of optical tweezers with positional detection in the back focal plane. *Rev Sci Instrum* 77:103101.
29. Schäffer E, Nørrelykke SF, Howard J (2007) Surface forces and drag coefficients of microspheres near a plane surface measured with optical tweezers. *Langmuir* 23:3654–3665.
30. Bormuth V, Varga V, Howard J, Schäffer E (2009) Protein friction limits diffusive and directed movements of kinesin motors on microtubules. *Science* 325:870–873.
31. Mickolajczyk KJ, et al. (2015) Kinetics of nucleotide-dependent structural transitions in the kinesin-1 hydrolysis cycle. *Proc Natl Acad Sci USA* 112:E7186–E7193.
32. Isojima H, Iino R, Niitani Y, Noji H, Tomishige M (2016) Direct observation of intermediate states during the stepping motion of kinesin-1. *Nat Chem Biol* 12:290–297.
33. Grant BJ, et al. (2011) Electrostatically biased binding of kinesin to microtubules. *PLoS Biol* 9:e1001207.
34. Hancock W (2016) The kinesin-1 chemomechanical cycle: Stepping toward a consensus. *Biophys J* 110:1216–1225.
35. Walker RA, Salmon ED, Endow SA (1990) The Drosophilaclaret segregation protein is a minus-end directed motor molecule. *Nature* 347:780–782.
36. Yajima J, Cross RA (2005) A torque component in the kinesin-1 power stroke. *Nat Chem Biol* 1:338–341.
37. Yajima J, Mizutani K, Nishizaka T (2008) A torque component present in mitotic kinesin Eg5 revealed by three-dimensional tracking. *Nat Struct Mol Biol* 15: 1119–1121.
38. Bugiel M, Böhl E, Schäffer E (2015) The kinesin-8, Kip3, switches microtubule protofilaments in a sideward random walk asymmetrically biased by force. *Biophys J* 108:2019–2027.
39. Kozielski F, et al. (1997) The crystal structure of dimeric kinesin and implications for microtubule-dependent motility. *Cell* 91:985–994.
40. Winding M, Kelliher MT, Lu W, Wildonger J, Gelfand VI (2016) Role of kinesin-1-based microtubule sliding in drosophila nervous system development. *Proc Natl Acad Sci USA* 113:E4985–E4994.
41. Bugiel M, et al. (2015) Versatile microsphere attachment of GFP-labeled motors and other tagged proteins with preserved functionality. *J Biol Meth* 2:e30.
42. Mahamdeh M, Schäffer E (2009) Optical tweezers with millikelvin precision of temperature-controlled objectives and base-pair resolution. *Opt Express* 17:17190–17199.
43. Bormuth V, Howard J, Schäffer E (2007) LED illumination for video-enhanced DIC imaging of single microtubules. *J Microsc* 226:1–5.